Article

Beyond Carbon Steel: Detecting Wellbore Shape and Cavities, and Cement Imperfections in Cased Wells

Timofey Eltsov *,† and Tadeusz W. Patzek

Ali I. Al-Naimi Petroleum Engineering Research Center, King Abdullah University of Science and Technology, Thuwal 23955-6900, Saudi Arabia; tadeusz.patzek@kaust.edu.sa

*   Correspondence: timofey.eltsov@kaust.edu.sa; Tel.: +966-1-2808-7182

†   Current address: 4700 KAUST, Thuwal, 23955-6900, Saudi Arabia.

check for updates

Abstract: The non-corrosive, electrically resistive fiberglass casing materials may improve the economics of oil and gas field projects. At moderate temperatures (<120 °C), fiberglass casing is superior to carbon steel casing in applications that involve wet CO_2 injection and/or production, such as carbon capture and storage, and CO_2-based enhanced oil recovery (EOR) methods. Without a perfect protective cement shell, carbon steel casing in contact with a concentrated formation brine corrodes and the fiberglass casing is superior again. Fiberglass casing enables electromagnetic logging for exploration and reservoir monitoring, but it requires the development of new logging methods. Here we present a technique for the detection of integrity of magnetic cement behind resistive fiberglass casing. We demonstrate that an optimized induction logging tool can detect small changes in the magnetic permeability of cement through a non-conductive casing in a vertical (or horizontal) well. We determine both the integrity and solidification state of the cement-filled annulus behind the casing. Changes in magnetic permeability influence mostly the real part of the vertical component of the magnetic field. The signal amplitude is more sensitive to a change in the magnetic properties of the cement, rather than the signal phase. Our simulations showed that optimum separation between the transmitter and receiver coils ranged from 0.25 to 0.6 m, and the most suitable magnetic field frequencies varied from 0.1 to 10 kHz. A high-frequency induction probe operating at 200 MHz can measure the degree of solidification of cement. The proposed method can detect borehole cracks filled with cement, incomplete lift of cement, casing eccentricity, and other borehole inhomogeneities.

Keywords: corrosion; magnetic cement; borehole measurements; electromagnetics; magnetic susceptibility

1. Introduction

According to the National Association of Corrosion Engineers ((NACE) https://www.nace.org/home), the total annual cost of corrosion in the oil and gas production industry is estimated to be $1.372 billion, broken down into $589 million in surface pipeline and facility costs, $463 million annually in downhole tubing expenses, and another $320 million in capital expenditures related to corrosion. As the oil and gas industry matures and it demands to sequester carbon dioxide at a massive scale, these corrosion costs may skyrocket. Luckily today, carbon steel casing tubulars can be replaced where appropriate with non-corrosive fiberglass composites.

Carbon steel casing corrodes quickly in a wet CO_2 environment [1,2] encountered in carbon capture and storage (CCS) and in CO_2-based improved and enhanced oil recovery processes. If a casing cement annulus is faulty or breaks down, the carbon steel corrodes when exposed to concentrated formation brine.

Talabani et al. [3] , Alcántara et al. [4], Sherar et al. [5], and Choi et al. [6] have found out that carbon steel casing may corrode by several mechanisms that act in series or in parallel. Most of these mechanisms are activated by the absence or imperfections of casing cement annulus or annuli for concentric casing strings.

- Erosion corrosion = wear/abrasion occurs at the casing surface during drilling and/or insertion of casing. Salts and oxides deposit or form at the casing surface, increasing localized corrosion;
- Hydrogen damage = hydrogen evolves on the cathodes on a chemically nonuniform steel casing and diffuses into the steel, leading to embrittlement and casing failure;
- Biological corrosion = local colonies of bacteria change chemistry across some regions of a casing surface; for example, sulfate reducing bacteria (SRB) form H_2S that corrodes the steel;
- Environmental corrosion = cement is absent and steel is exposed to concentrated chlorides in a formation brine or across overlying aquifers;
- Galvanic corrosion = cement is absent and electrolyte is present between two dissimilar casings which connect electrically and one becomes the anode.

A special case is the corrosion of cased horizontal well laterals. The displacement of drilling fluid from high-angle and horizontal wellbores is complicated, and cement integrity is uncertain and often impaired [7]. Therefore, an exposed horizontal well casing may be subject to most of the corrosion mechanisms described above. In addition, with poor cement quality, horizontal well refracturing is problematic [8].

The evaluation of cement integrity is of primary importance to the oil and gas industry [9]. Poor cementation can lead to costly accidents and serious damage to the environment. According to a BP report [10], one of the reasons for the Macondo well blowout on 20 April 2010, was poor zonal isolation with a foam cement. Thus, cement placement and the evaluation of cement quality must both be improved. Magnetic particles are used in different applications. They enable various tasks to be performed remotely. In medicine, these particles are used for drug delivery systems, cancer diagnosis, or bioseparation [11]. In the oil industry, they are used for hydraulic fracture evaluation, EOR, and other applications [12]. The magnetorheological approach can be used to inject cement slurry uniformly into an annular space between the casing and borehole wall. Magnetic cement slurry can be displaced into regions where it would not otherwise flow when pumped conventionally [13]. Magnetic properties of cement change with time because of heating and aging. Electrical properties of a cement-based magnetorheological fluid differ from those of common cement. The presence of conductive particles increases the magnetic permeability of the cement [14] and, because of the proximity of the cement-filled annulus to casing, one can use the magnetic susceptibility logging method to determine cement quality. It is necessary to estimate the magnitude of the useful signal and quantify appropriate measurement methods. This leads to an accuracy assessment of the sensors or magnetometers that should be installed in the magnetic cement sensing tool. A thorough analysis of the available sensors and frequency ranges helped us compile Figure 1. Measurement of electromagnetic fields for geophysical purposes covers a wider range than those required by most of the other fields. For example, when performing cross-well EM exploration, the noise level was estimated as 0.5×10^{-5} nT [15]. The magnitudes of magnetic fields used in cardiac or brain medical research are also very small and require precise and expensive equipment. We do not need such a high accuracy for assessing the quality of magnetic cement as flux-gate magnetometers, Hall-effect sensors, or solenoid type sensors are quite sufficient.

Measuring electrical properties through casing was a great challenge in the second part of the last century. The complex effects of casing were captured long ago and solutions were found [16,17], providing two methods of logging in cased wells. Due to the high conductivity of steel casing relative to the surrounding formation, the expected measurements are to be made in the nanovolt range [18]. Technical and computing capabilities of the industry in the 1940s were insufficient for such precise measurements. Kaufman [19] developed a theory of measuring formation resistivity in a cased borehole

with a sufficient accuracy for practical applications. Schlumberger has implemented the theory and provides the formation resistivity log in a cased borehole called CHFR [18,20]. This log takes about 12 h to run, with each measurement consuming about 2 min. There are theoretical preconditions for logging through the casing on the basis of magneto-acoustic effects [21,22]. It is proposed to estimate electrical properties from an acoustic signal generated by a sensor responding to acoustic waves at a metal surface in communication with an earth formation. The metal surface is exposed to a constant magnetic field normal to it and a harmonic magnetic field of variable frequency along the surface. Further development of this method requires additional laboratory experiments.
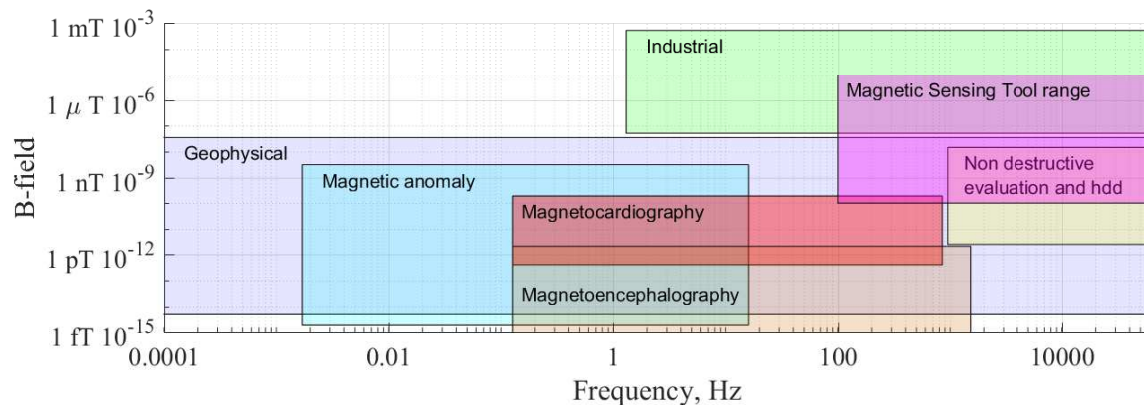

Figure 1. Magnetic field ranges and frequencies used in different disciplines, compiled after Ripka [23]. The range of B-field magnitude and frequency used in the numerical experiments discussed in this paper is marked in magenta.

Existing methods of estimating electrical properties behind casing are not suitable for the assessment of electrical properties of cement. These methods evaluate the integral electrical formation properties at a distance away from the casing or are currently underdeveloped. In this paper, we propose a tool to measure and control the integrity of a weakly magnetic cement behind non-conductive fiberglass casing. The objective is to verify cement quality in a borehole environment by computing the tool parameters such as distance between coils and operating frequencies. Borehole environment is magnetized by a low frequency induction tool. Measurements can be made with a set of coils or sensors. The alternating magnetic field provides necessary noise immunity for logging and excludes the influence of the geomagnetic field [24]. Significant work has been devoted to studying the influence of borehole media's electrical properties on electromagnetic logging signals, for example the dielectric permeability and its distribution [25], or change of electrical resistivity of the invaded zone [26]. The effect of magnetic permeability on the inductive response has been studied for metal detector applications [27] and logging applications [28,29]. However, cement detection and the measurement of cement integrity have not been studied sufficiently for weakly magnetic cements. Here we focus on detecting small changes in the magnetic permeability of a cement-filled annulus behind a non-conductive casing.

2. Theory and Method

To simulate magnetic susceptibility logging, we solved the Maxwell equations of electromagnetism [30] in cylindrical coordinates. Transmitter coil generates a primary magnetic field that produces an eddy current in the formation, see Figure 2. The primary and secondary magnetic fields induce an electromotive force in the receiver coil. Only the vertical component, H_z, of the magnetic field is considered. Key model assumptions are:

- The system consists of 4 concentric cylinders—wellbore, casing, cement, and formation – with constant electrical properties along the *z*-axis;

- All layers are isotropic and homogeneous;
- The wellbore is an infinite column of liquid and its axis coincides with the common axis of all cylinders;
- Coil axes coincide with the wellbore axis, and;
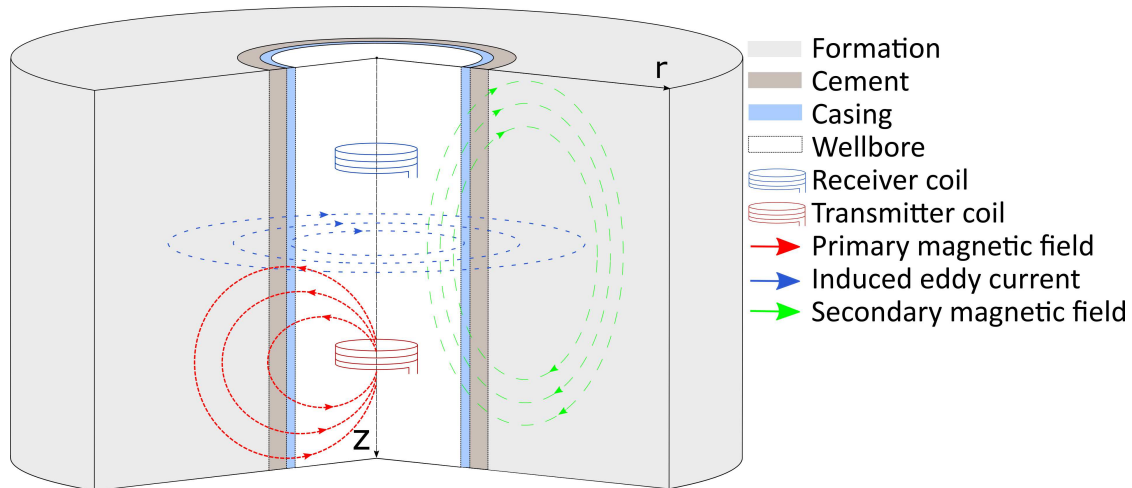- Compared with the tool size, coils are small and can be approximated by point dipoles.

Figure 2. Schematic representation of an idealized geoelectric system.

Signals are obtained from a solution of the Helmholtz equation in cylindrical coordinates (r, φ, z):

$$\frac{1}{r}\frac{\partial}{\partial r}\left(r\frac{\partial A_z}{\partial r}\right) + \frac{1}{r^2}\frac{\partial^2 A_z}{\partial \varphi^2} + \frac{\partial^2 A_z}{\partial z^2} + k^2 A_z = 0, \tag{1}$$

$$H_z = k^2 A_z + \frac{\partial^2 A_z}{\partial z^2}, \; H_r = \frac{\partial^2 A_z}{\partial r \partial z}, \; E_\varphi = i\omega\mu\frac{\partial A_z}{\partial r}, \tag{2}$$

$$k_m{}^2 = -i\omega\mu_m(\sigma_m - i\omega\epsilon_m), \tag{3}$$

where A_z is the vector potential; ω is the angular frequency; $\mu_m = \mu_{r,m}\mu_0$, the magnetic permeability ($\mu_{r,m}$—relative, μ_0—permeability of vacuum, m–the layer index); σ_m is the electrical conductivity; and ϵ_m is the dielectric permittivity ($\epsilon_m = \epsilon_r\epsilon_0$, r—relative, 0—permittivity of vacuum). Since at low frequencies, the contribution of the dielectric constant is negligible, the relative permittivity of all layers is set to 1.

The vector potential in the wellbore is:

$$A_{z,1}(r,z) = \frac{M}{4\pi}\left(\frac{e^{-ik_1 R}}{R} + \frac{2}{\pi}\int_0^\infty C_1 I_0(\lambda_1 r)\cos\lambda z \, d\lambda\right), \tag{4}$$

$$\lambda_m = \sqrt{\lambda^2 + i\sigma_m\mu_m\omega}, \; R = \sqrt{r^2 + z^2} > 0. \tag{5}$$

Here M is the magnetic moment of the coil; λ is the separation variable; r the radial distance; z the axial distance; k_1 is the wave number corresponding to the borehole; and C_1 is a constant that carries information about the borehole environment and is obtained from the boundary conditions that require the continuity of the tangential components of the electric, E_φ, and magnetic, H_z, field. Using these conditions, we solve a system of linear Equation (2). The solution allows us to determine the distribution of the electromagnetic field in the wellbore and translate this field into measured signals.

The measured signals are the phase, φ_m, and the amplitude, A_m, of the electromotive force induced by the magnetic field in the receiving coil:

$$a = Re(H_z), \quad b = Im(H_z), \tag{6}$$

$$\varphi_m = \arctan\left(\frac{b}{a}\right), \quad A_m = \sqrt{a^2 + b^2}. \tag{7}$$

The logging signals are often displayed in apparent resistivity that itself is a well-known physical property of the rock. In Section 3.3 we show that measuring apparent resistivity allows us to detect cement solidification using a 200 MHz induction tool. We use a homogeneous medium approximation to calculate the apparent electrical resistivity from signal amplitude. The apparent resistivity calculation algorithm was described in [31]. There are many ways to transform signals into apparent resistivities, e.g., the pallet method, optimization methods, and asymptotic formulæ. To convert signals into apparent resistivities, we chose the Newton method for efficiency. A good initial guess is necessary to ensure convergence in a small number of iterations when using this method. The exact formulæ for calculating induction logging signals, Equation (7), have been transformed, and a good initial guess has been constructed. The apparent resistivity calculation algorithm used here is accurate to at least six significant digits.

The electrical properties of the media are listed in Table 1. Wellbore, which passes through a carbonate formation, was filled with a fresh water-based mud. The well was cased with a fiberglass casing. The magnetic permeability of cement depends on the concentration of iron powder in it. Using an analytical solution, we varied the frequency, f, magnetic moment of the source, M, the electrical conductivity of the drilling mud and the surrounding rock, σ, and the magnetic permeability of cement, μ. The magnetic permeabilities varied between 1 and 2. This variation corresponds to the magnetic particle content from 0% to 15% as a volume fraction, according to [32]. In addition, we varied the distance between the receiver and the source, z, in order to choose the most optimal configuration of the magnetic logging tool.

We have confirmed the analytical solution by the finite element method using COMSOL Multiphysics® 5.2. Unlike the analytical solution, in which there are no boundaries perpendicular to the wellbore, COMSOL allowst the study of the influence of such heterogeneities on the logging signals. We considered various logging scenarios detailed in Section 3.3: Incomplete lift of cement, cement debonding, cavities, fractures, and other inhomogeneities. We used parameters from Table 1 and varied the position of the transmitter by a step of 1 cm down the wellbore. The distance between the transmitter and receivers remains unchanged.

Table 1. Geoelectric model parameters.

Parameter	Wellbore	Fiberglass Casing	Cement	Formation
Radius, m	0.07	0.10	0.15	
Resistivity, $\Omega \cdot$m	2	10^8	100	50
Magnetic permeability	1	1	1, 1.25, 1.5, 2	1

Apparent Magnetic Permeability

Our calculation of apparent magnetic permeability is based on the assumption of the medium's homogeneity. A change in the real part of magnetic field is proportional to the change of medium's magnetic permeability. It is worth describing the calculation of geometrical and demagnetization coefficients, as they determine the conditions of measurements. In a homogeneous environment, these coefficients are expressed as [24]:

$$G\text{æ}' = \frac{\xi_{z,s} + \xi_{z,p}}{\xi_{z,p}}, \quad \text{æ}' = \frac{\text{æ}'}{(1 + N\text{æ})}. \tag{8}$$

Here $æ'$ is the apparent magnetic susceptibility, ($\mu_{apparent} = 1 + æ$); G, the geometrical coefficient; ζ, the electromotive force; N, the demagnetization factor; and p and s denote the primary and secondary field indices. The imaginary part for the preferred frequency range in Figure 3 is negligible when compared with the real part. In this case, the amplitude is equal to the modulus of the real part of the magnetic field, see Equation (7).

Magnetic susceptibility can be expressed as:

$$\frac{æ}{1 + Næ} = \frac{\zeta_{z,s} + \zeta_{z,p}}{G\zeta_{z,p}}, \quad \zeta = i\omega\mu\sigma H_z. \tag{9}$$

where $æ$ is the magnetic susceptibility of the medium. From a general solution of the boundary value problem, and in accordance with Equation (8), we obtain the geometrical and demagnetization coefficients:

$$G = \lim_{æ \to 0} \frac{\zeta_{z,s} + \zeta_{z,p}}{æ\zeta_{z,p}}, \quad N = \frac{G\zeta_{z,p}}{\zeta_{z,s} + \zeta_{z,p}} - \frac{1}{æ}. \tag{10}$$

These coefficients can be calculated from experimental data by solving a system of linear equations:

$$\frac{\zeta_{z,s} + \zeta_{z,p}}{æ\zeta_{z,p}}(1 + Næ_i) = Gæ_i, \quad i = 1, 2, \dots \tag{11}$$

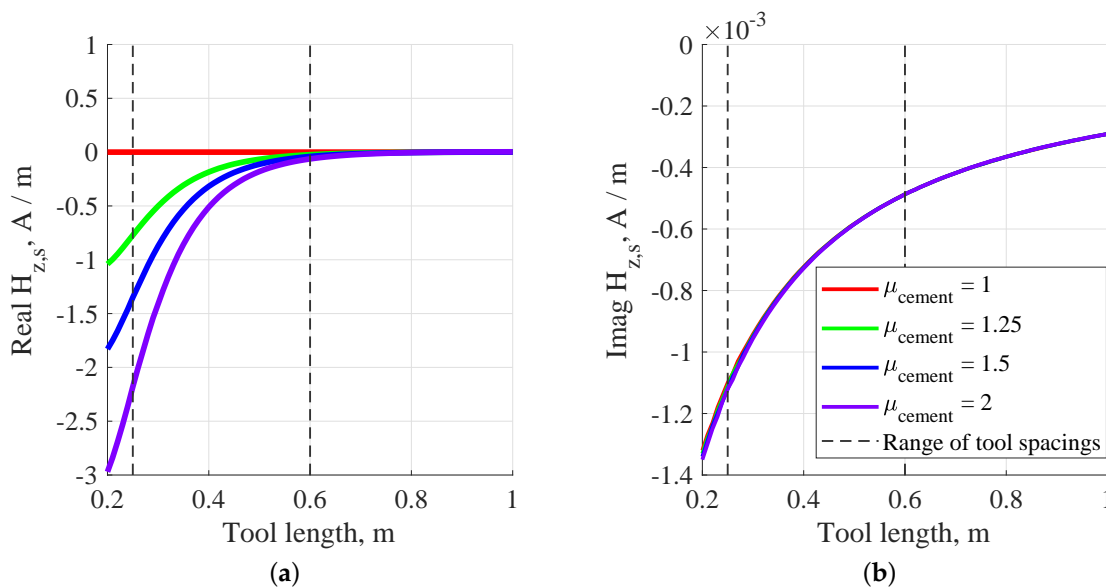Here i is the subscript of the medium with the magnetic susceptibility $æ_i$.

Figure 3. Effect of magnetic permeability of cement on magnetic field at the frequency of 1 kHz: (**a**) Tool length vs. real part of secondary field, $H_{z,s}$. (**b**) Tool length vs. imaginary part of $H_{z,s}$.

3. Results

To understand the signals that should be used to extract magnetic properties of a composite medium, it is necessary to analyze the magnetic field itself, as well as the response of the medium under study. We assume that the tool is properly calibrated, i.e., the primary magnetic field has been excluded from the measurements. Figure 3 shows that the real part of the secondary field, $H_{z,s}$, is three orders of magnitude stronger than the imaginary part. Smaller spacings between coils enhance the detection of the magnetic permeability of the cement and the distance between the coils ought to be 25–60 cm (dashed line) to optimize this detection.

We have modeled the magnetic tool responses to changes in the drilling fluid resistivity, formation resistivity, cement hardening, and magnetic permeability of the cement (amount of magnetic

particles). The amount of magnetic powder in the cement has a strong influence on the real part of the secondary field, $H_{z,s}$, i.e., useful information about cement integrity can be extracted from it. Curves for the different resistivities of cement, mud, and formation overlap. Changes in the frequency of the transmitter coil in the lower part of the kHz range do not significantly affect the real part of $H_{z,s}$. At the same time, changes in frequency affect the imaginary part of $H_{z,s}$ more strongly in the upper kHz range. With an increasing frequency, the amplitude of the imaginary part of $H_{z,s}$ grows and becomes the same order as that of the real part. To simplify measurements and processing, we suggest using the lower part of the kHz range. In this case, there is no significant effect of the imaginary part of the magnetic field. Therefore, we propose the use of frequencies ranging from 0.1 to 10 kHz, typical of magnetic susceptibility logging. A typical pattern of $H_{z,s}$ vs. tool length is presented in Figure 3.

Figure 4 shows that the signal amplitude is suitable for extracting magnetic properties of cement. Simulation results presented in Figure 3 and Equation (7) support this conclusion. The signal amplitude is insensitive to cement resistivity, i.e., to cement rheology in the frequency range from 0.1 to 10 kHz. Signal simulations for different configurations of borehole geometry show that the singularities of the signal phase are caused by the magnetized cement and its distance from the measurement point.
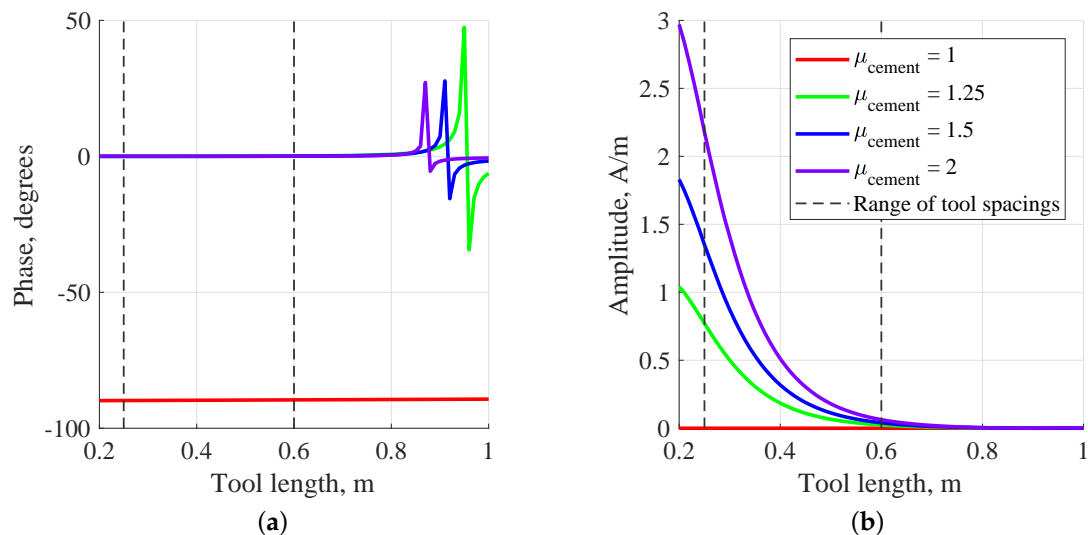

Figure 4. Effect of magnetic permeability of cement on induction logging signals at the frequency of 1 kHz: (**a**) Phase vs. tool length. (**b**) Amplitude vs. tool length.

Apparent magnetic permeability in Figure 5 differs from the actual permeability of magnetic cement because only a part of the medium is magnetic. In Figure 4b, the apparent magnetic permeability has been calculated from the signal amplitude. Finally, short tools are more sensitive to the magnetic properties of cement.
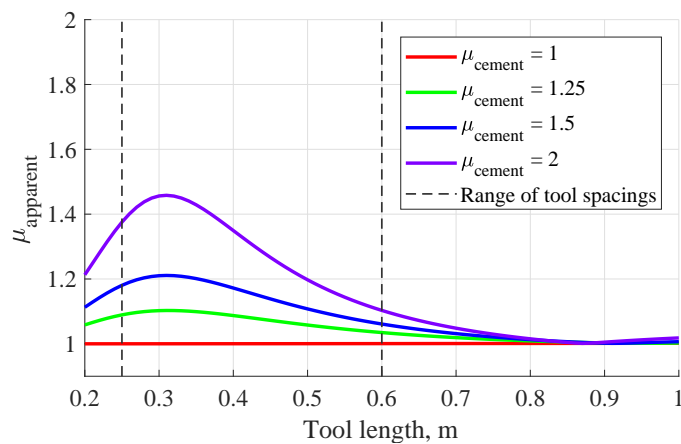
Figure 5. Apparent magnetic permeability vs. tool length at the frequency of 1 kHz.

3.1. Sensing Solidification of Concrete

It is known that the electrical resistance of cement depends on the degree of its solidification. The electrical resistivity of cement grows as it solidifies [33]. The rate of resistivity increase depends on water fraction in the cement paste or foam, water conductivity, and other parameters. These questions go beyond our research objectives, because here we only need to know the aggregate state of cement. For simplicity, it can be said that the cement paste has an electrical resistance below 5 Ohm·m. Cement with a resistivity >50 Ohm·m might be considered solid. It reaches this resistance in several hours and with time the resistance slowly grows [34]. This raises the following question: How can one detect a relatively conductive cement-filled annulus behind a non-conducting casing? Methods for measuring DC resistance are not suitable for this task. Fiberglass casing is a resistor and current will not flow through it. To measure cement resistance, one can use a high frequency induction method. The high frequency EM field weakly damps in the insulator and penetrates into the cement annulus. The best results can be achieved by pressing the tool against the casing wall. This is necessary to minimizes signal losses in drilling mud.

The imaginary part of the magnetic field intensity detects changes of cement resistivity. Figure 6 shows the imaginary part of the secondary magnetic field versus distance between the transmitter and receiver. The source is a point dipole oscillating at the frequency of 200 MHz. The geometric and electric parameters are listed in Table 1. The relative magnetic permeability of the cement is 1.5. In this case, a two-coil tool and a three-coil tool can be used. It is recommended that tools with a separation between coils ranging from 0.3 to 0.4 m are used. We conclude that soft cement can be detected at a high frequency.
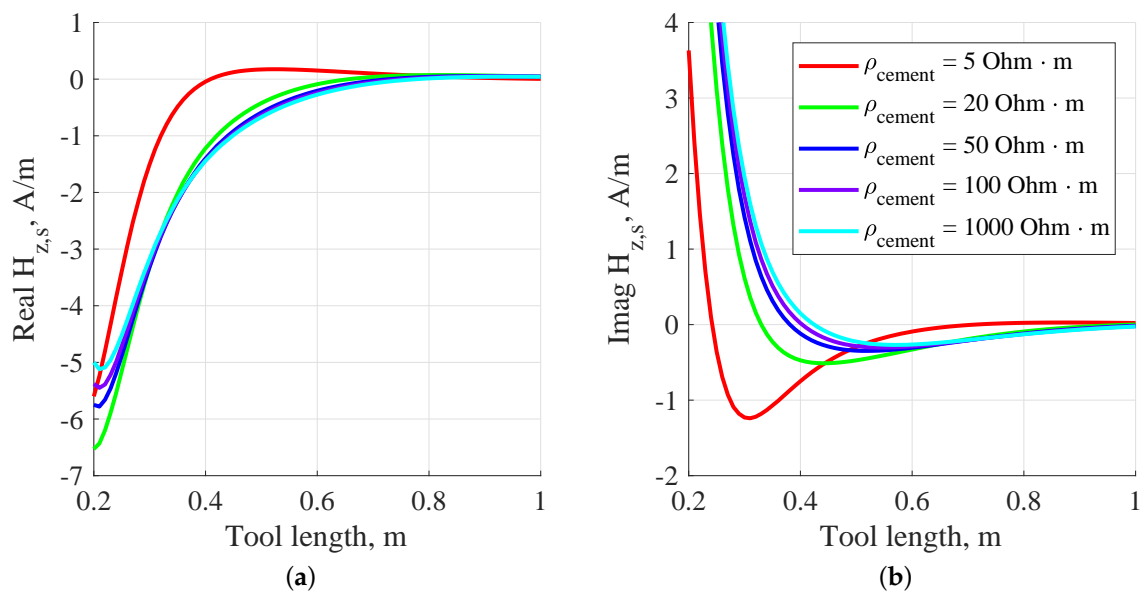
Figure 6. Intensity of (**a**) real and (**b**) imaginary part of $H_{z,s}$ vs. tool length at the frequency of 200 MHz. Different state of the cement is considered: The harder the cement, the higher the resistivity.

3.2. The Analytic Solution Versus the Finite Element Method

COMSOL software calculations and analytic solutions were identical, see Figure 7a. We considered a point magnetic dipole, oscillating at the frequency of 1 kHz. The dipole was located at the origin, the length of the well was 3 m, the diameter of the model was 3 m, and the geometric and electrical parameters of the model are from Table 1. The nonuniform mesh parameters used in the modeling are: the maximum element size = 1 cm and the minimum one = 8×10^{-5} m. Maxwell's equations are solved in the frequency domain, and the number of degrees of freedom is 1,199,956. The external boundary is assumed to be a magnetic and electric insulator. Due to the short length of the probes relative to the model size, the influence of the external boundary can be neglected. Simulations were carried out in two environments to obtain the secondary magnetic field, i.e., air and the medium under study. The response in the air was subtracted, i.e., the tool response was calibrated. The signals were calculated using Equation (7). The signals computed with the finite element method were less smooth than those from the analytical calculations. Despite the very fine mesh, the COMSOL-computed signals were rough, see Figure 7a. Increasing the element sizes further reduced the accuracy of the calculation. The magnetic field strength scale was amplified in Figure 7b to improve visualization of the field distribution. Relative to a non-magnetic medium, a magnetic cement with μ = 2 is practically a "magnetic conductor".
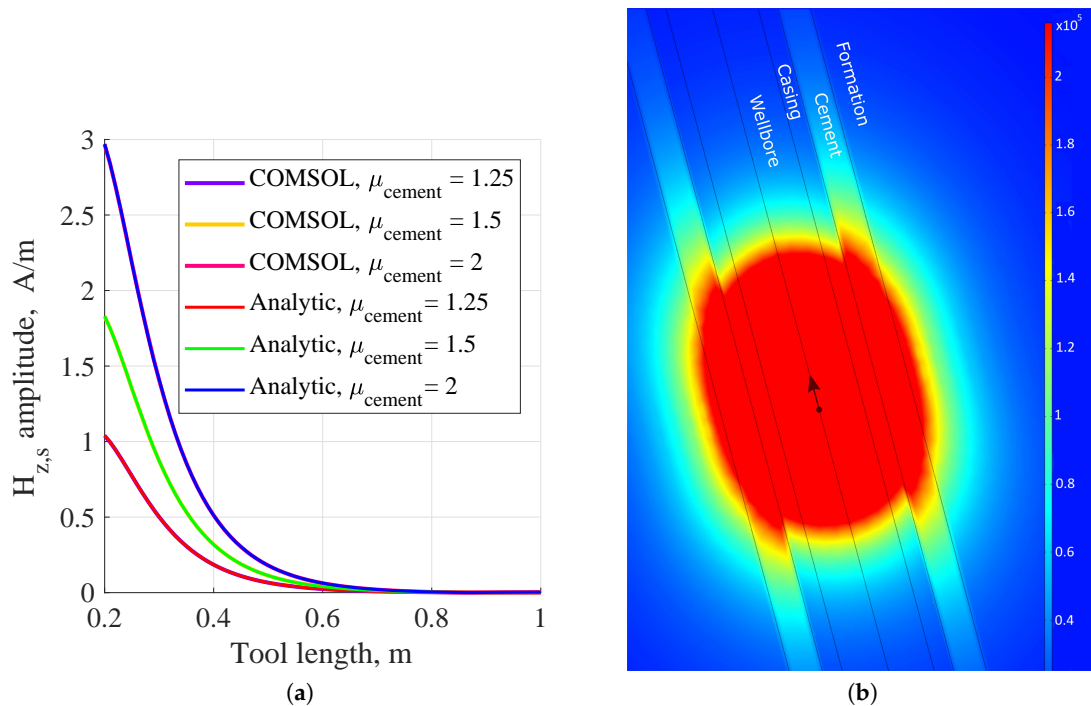
Figure 7. (**a**) Comparison of useful signal amplitude computed using COMSOL and analytic solution and (**b**) propagation of the magnetic field generated by a point dipole source in the wellbore at the frequency of 1 kHz (COMSOL).

3.3. Logging Signal Modeling

To test the technology being developed, we performed numerical testing of magnetic logging for five scenarios: (1) Incomplete lift of cement, (2) cavity, (3) crack filled with magnetic cement, (4) 2 cm cement debonding, and (5) progress of cement solidification along the borehole. The 2D axisymmetric simulations were performed using the AC/DC module in COMSOL. The source of electromagnetic waves was a point dipole with the magnetic moment = 1 A·m^2. The dipole oscillates was at the frequency of 1 kHz for scenarios 1–4. The magnetic moment was 0.1 A·m^2 and the frequency was 200 MHz for the 5th scenario. Probes with the lengths of 30, 35, 40, and 50 cm passed through a wellbore interval with inhomogeneities. The geometric and electric parameters are listed in Table 1. The relative magnetic permeability of the cement was 1.5. Response in the air was subtracted. For the 5th scenario, six different cement resistivities were used to depict its solidification: 1, 5, 20, 50, 100, and 1000 Ohm·m. In this case, cement tubes that were 1 m high lay on top of each other, and the space above 1 Ohm·m tube was filled with air. For the cement solidification state, an additional 25 cm long tool was considered because at high frequencies the skin depth, ($\delta = \sqrt{\frac{2}{\sigma \mu \omega}}$, σ being the electrical conductivity) significantly decreased.

Figure 8a,b show that an incomplete rise of cement could be determined by an abrupt decrease of amplitude of the secondary magnetic field. Figures 8c,d and 9a,b demonstrate that the proposed tool was capable of detecting cement inhomogeneities and it was more sensitive to the near wellbore region. The shape and intensity of magnetic logging curvesweare determined by the shapes of heterogeneities filled with cement. Cement adjacent to the well casing generated the strongest tool response. An absence of cement resulted in a sharp decrease of magnitude of the secondary magnetic field observed in Figure 9c,d.
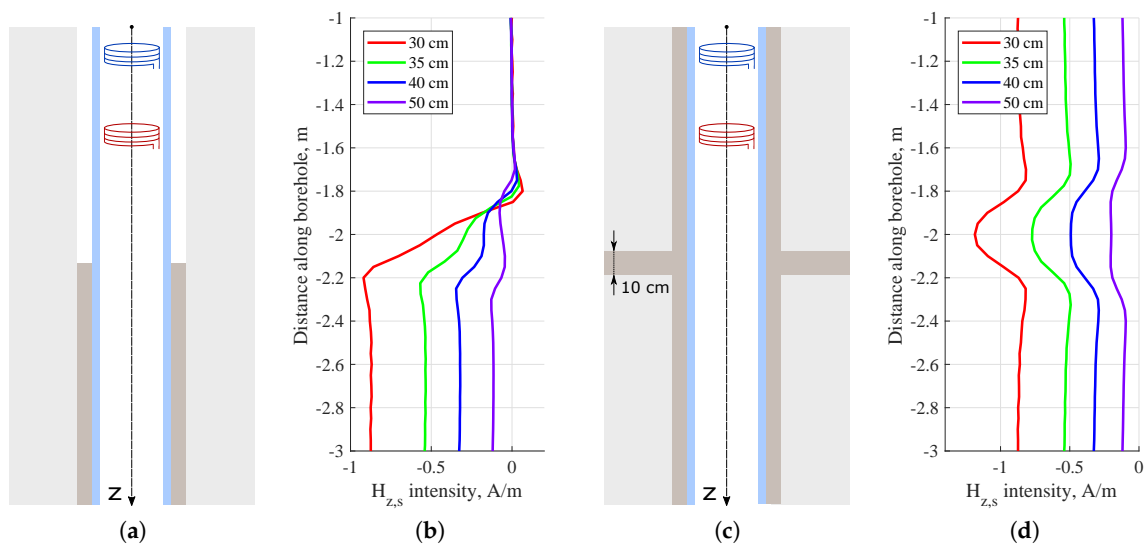
Figure 8. (**a**) The model of an incomplete lift of cement, (**b**) logging signals at the frequency of 1 kHz cross a cement lift, (**c**) the model crack filled with magnetic cement, and (**d**) logging signals at the frequency of 1 kHz cross a crack filled with magnetic cement with different tool lengths considered.
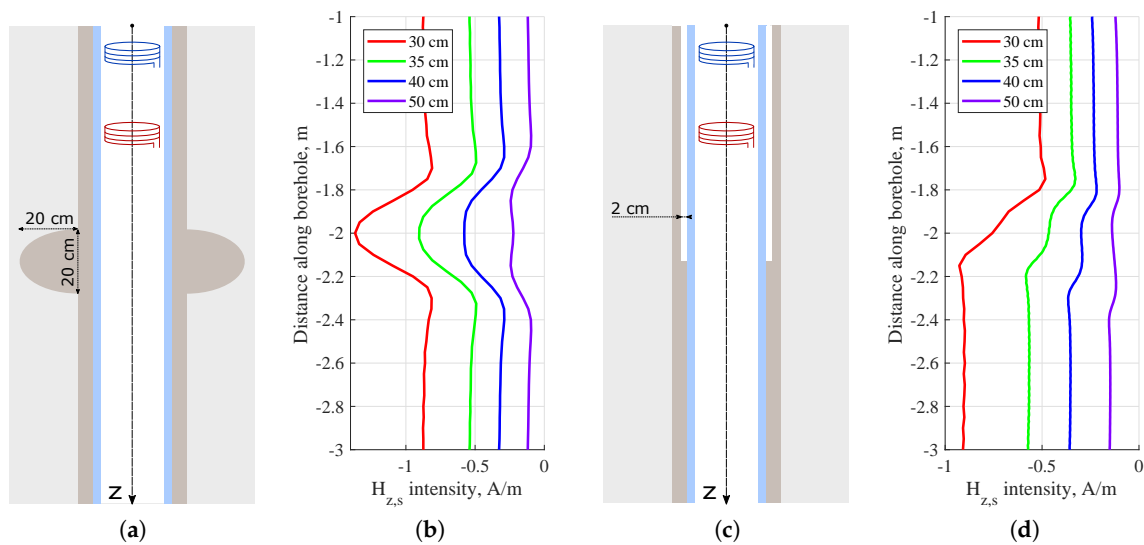

Figure 9. (**a**) The model of a cavity filled with a cement, (**b**) logging signals at the frequency of 1 kHz cross a cavity filled with cement, (**c**) the model of a cement with 2 cm debonding, and (**d**) logging signals at the frequency of 1 kHz cross a debonding area.

When logging at 200 MHz, see Figures 10 and 11, one can observe a stair-step change of the real and imaginary part of $H_{z,s}$. It is important to note that in this particular case, magnitudes of the imaginary and real parts of $H_{z,s}$ were very close and the stair-step changes were opposite for both components. Figure 11 shows that we can easily distinguish a "liquid" cement (1–5 Ohm·m) from a "solidified" cement (50 Ohm·m and more). It is impossible to distinguish a 50 Ohm·m layer from a 100 Ohm·m one, but a trend of solidification can be observed. Short tools are more sensitive to the wellbore and measured the lowest resistivities. Longer tools better sensed the near-wellbore space. Due to the special nature of the electromagnetic field and model complexity, the electrical resistances calculated from the phase, Figure 11b, and amplitude, Figure 11c, differed significantly. For a better display, Figure 11b is plotted as dots because the boundary-related singularities in the resistivity log obtained from the signal phase obscure the tool responses. However, compared with the amplitude, the signal phase was more sensitive to the cement solidification state. The effect of surrounding layers was more significant for the graph generated from amplitude rather than those from the signal phase.
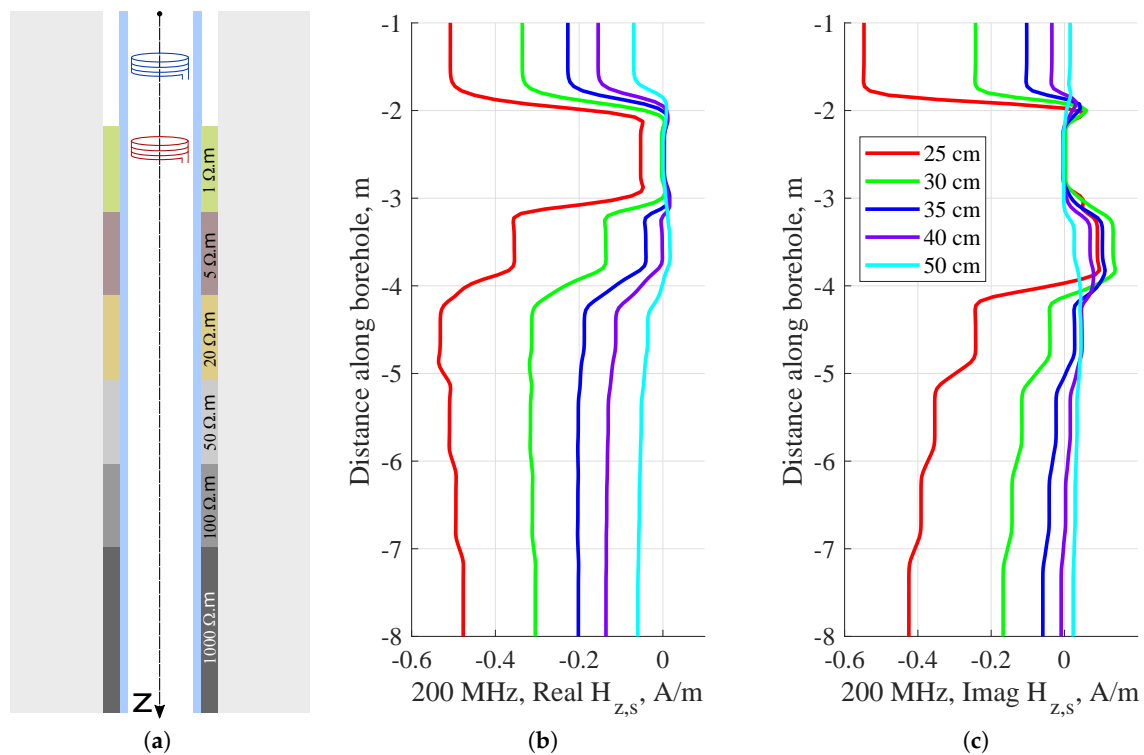

Figure 10. (**a**) The wellbore model with different resistivities of the cement (different solidification states) and induction logging signals at the frequency of 200 MHz for (**b**) real and (**c**) imaginary part of $H_{z,s}$. Different tool lengths are considered.

Simulations show that the zones with insufficient cementing could be easily determined using the proposed tools, a high-frequency induction tool could be used to distinguish between the zones of "solidified" and "liquid" cement.
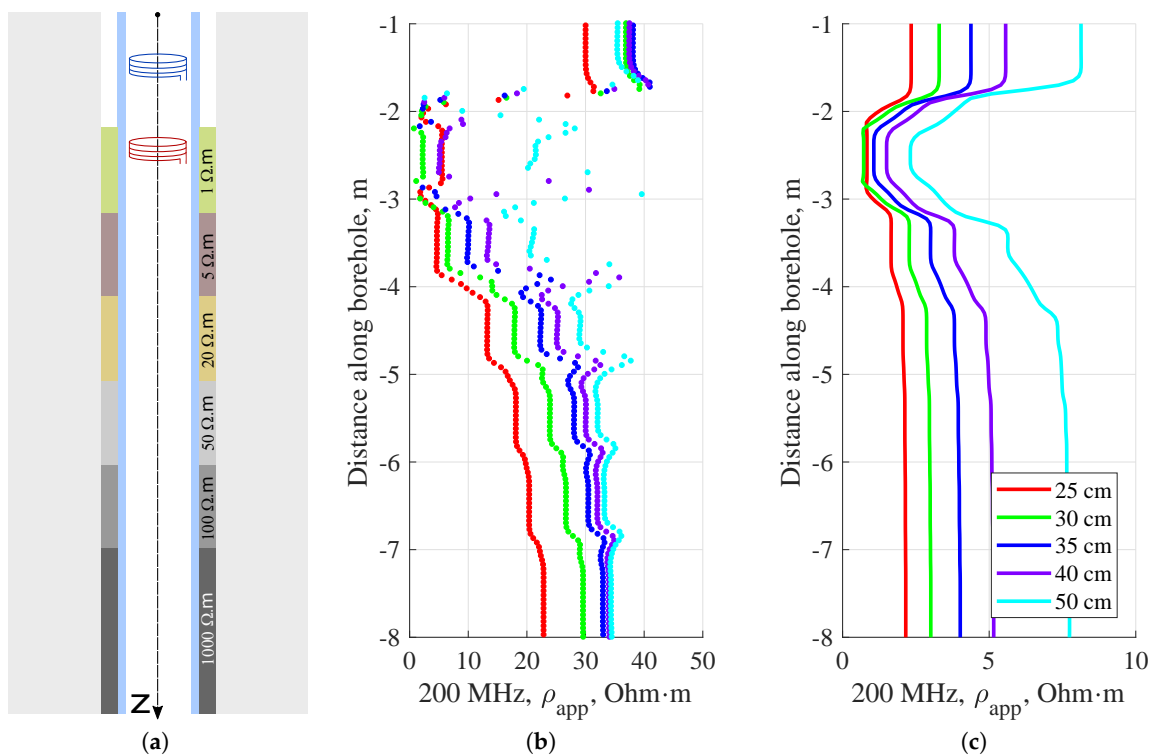
Figure 11. (**a**) The wellbore model with different resistivities of the cement (different solidification states) and apparent resistivity at the frequency of 200 MHz calculated from (**b**) signal phase and (**c**) amplitude. Different tool lengths are considered.

3.4. Detection of Radial Inhomogeneities

Magnetic logging signals were simulated to study the possible detection of radial inhomogeneities: (1) The eccentricity of the cement, and (2) a crack filled with the magnetic cement. The 3D simulations were performed using the AC/DC module in COMSOL. The model was a 1.5 m long cylinder with a diameter of 1.5 m. The complete mesh consisted of 1,387,193 domain elements, 65,048 boundary elements, and 2327 edge elements. The average element quality was 0.7679. The source of electromagnetic waves was a point dipole with the magnetic moment of 1 A·m^2, oscillating at the frequency of 1 kHz in the middle of the borehole. The external boundary was assumed to be a magnetic and electric insulator. The distances between the transmitter and receivers were 30, 35, 40, and 50 cm. The influence of the outer boundary was neglected. The magnetic field was registered by 12 sensors evenly distributed inside the casing, see Figures 12 and 13. The geometric and electric parameters are listed in Table 1. The relative magnetic permeability of the cement was 1.5. The tool response was calibrated by subtracting the system response in the air. Figure 12 shows that an asymmetric distribution of magnetic cement can be detected by the proposed tool. Figure 13 shows that a small radial crack filled with cement was invisible to the tool. The distance to the crack was too large and the contribution to the signal from the anomaly was less than the tool's measurement error. However, insufficient cementation near the casing could be detected with magnetic logging signals.
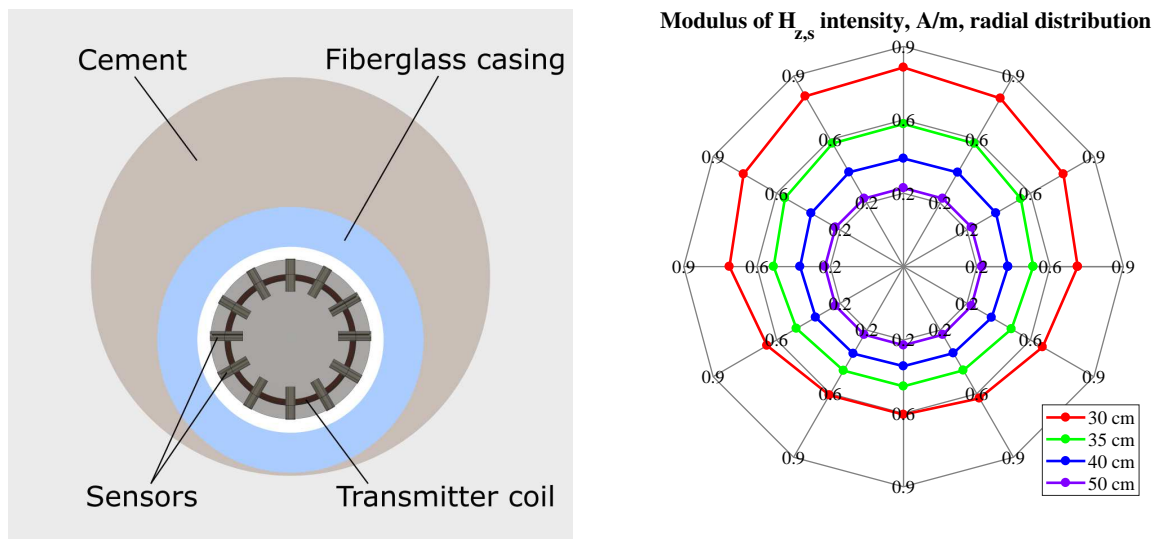
Figure 12. Facet of eccentric wellbore filled with magnetic cement. The signal frequency is 1 kHz.
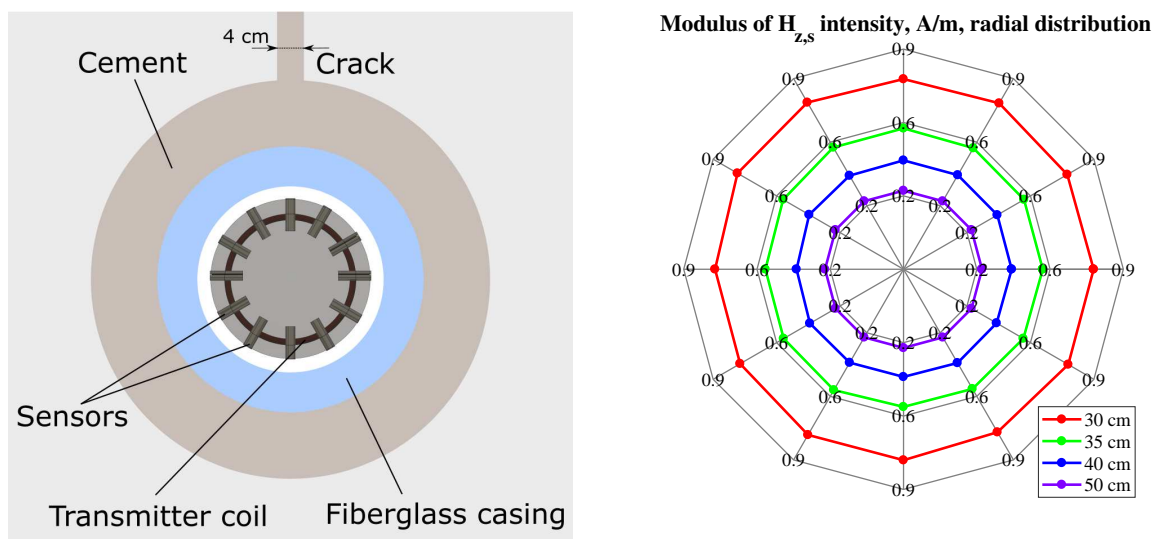

Figure 13. Facet of wellbore and crack filled with magnetic cement. The signal frequency is 1 kHz.

4. Conclusions

We optimized an induction logging tool for testing the integrity of a weakly magnetic cement behind a non-conductive casing. Tools with the lengths of 0.25–0.6 m were most sensitive to magnetic cement properties. The real part of the secondary magnetic field, $H_{z,s}$, was more sensitive to magnetic cements than the imaginary part. The most suitable frequencies for magnetic cement detection were in the range of 0.1 to 10 kHz, typical of magnetic susceptibility logging. Amplitude could be used to infer the integrity of the magnetic cement behind the casing, but to obtain information about cement rheology, it was necessary to perform the high-frequency resistivity measurements. Logging at 200 MHz distinguished solid cement from liquid and quantified the cement solidification state. Signal phase at a high frequency was more sensitive to cement solidification, rather than amplitude. Cavities and cracks filled with magnetic cement were visible on the logs. The proposed tool could be used for the determination of the zones of cement debonding. Casing eccentricity and radial inhomogeneities could be detected using the radially distributed sensors. The absence of cement caused a sharp decrease of the magnitude of the secondary magnetic field. The magnetic logging

technology proposed in this paper could be used to check cement quality in moderate temperature wells (<150 °C). The proposed method could determine poor zonal isolation and cement hardening.

Abbreviations

AC	Alternating current
CCS	Carbon Capture and Storage
CHFR	Cased-hole formation resistivity
DC	Direct current
EM	Electro-magnetic
EOR	Enhanced oil recovery
Imag	Imaginary part
SRB	Sulfate reducing bacteria

References

1. Watson, T.L.; Bachu, S. Evaluation of the potential for gas and CO_2 leakage along wellbores. *SPE Drill. Complet.* **2009**, 115–126. [CrossRef]
2. Jia, B.; Tsau, J.S.; Barati, R. A review of the current progress of CO_2 injection EOR and carbon storage in shale oil reservoirs. *Fuel* **2019**, *236*, 404–427. [CrossRef]
3. Talabani, S.; Atlas, B.; Al-Khatiri, M.; Islam, M. An alternate approach to downhole corrosion mitigation. *J. Petroleum Sci. Eng.* **2000**, *26*, 41–48. [CrossRef]
4. Alcántara, J.; de la Fuente, D.; Chico, B.; Simancas, J.; Díaz, I.; Morcillo, M. Marine atmospheric corrosion of carbon steel: A review. *Materials* **2017**, *10*, 406. [CrossRef] [PubMed]
5. Sherar, B.; Power, I.; Keech, P.; Mitlin, S.; Southam, G.; Shoesmith, D. Characterizing the effect of carbon steel exposure in sulfide containing solutions to microbially induced corrosion. *Corros. Sci.* **2011**, *53*, 955–960. [CrossRef]
6. Choi, Y.S.; Young, D.; Nesic, S.; Gray, L.G. Wellbore integrity and corrosion of carbon steel in CO_2 geologic storage environments: A literature review. *Int. J. Greenh. Gas Control* **2013**, *16S*, 70–77. [CrossRef]
7. Sabins, F.L. Problems in cementing horizontal wells. *J. Pet. Technol.* **1990**, *42*, 398–400. [CrossRef]
8. Cameron, J. Refracturing horizontal shale wells with solid-steel expandable liners. *World Oil* **2013**, *234*, 39–52.
9. Eltsov, T.; Patzek, T. Beyond Steel Casing: Detecting Zonal Isolation in the Borehole Environment. In Proceedings of the SPE Middle East Oil and Gas Show and Conference, Manama, Bahrain, 18–21 March 2019.
10. BP. *Deepwater Horizon Accident Investigation Report*; Technical Report; BP: Washington, DC, USA, 2010.
11. Ito, A.; Shinkai, M.; Honda, H.; Kobayashi, T. Medical Application of Functionalized Magnetic Nanoparticles. *J. Biosci. Bioeng.* **2005**, *100*, 1–11. [CrossRef] [PubMed]
12. Guo, K.; Li, H.; Yu, Z. Metallic nanoparticles for enhanced heavy oil recovery: Promises and challenges. *Energy Procedia* **2015**, *75*, 2068–2073. [CrossRef]
13. Nair, S.D. Adaptive Performance of Cement-based Materials Using a Magnetorheological Approach. Ph.D. Thesis, The University of Texas at Austin, Austin, TX, USA, 2013.
14. Nair, S.D.; Ferron, R.D. Real time control of fresh cement paste stiffening: Smart cement-based materials via a magnetorheological approach. *Rheol. Acta* **2016**, *55*, 571–579. [CrossRef]
15. Marsala, A.F.; Lyngra, S.; Safdar, M.; Zhang, P.; Wilt, M. Crosswell electromagnetic induction between two widely spaced horizontal wells: Coiled-tubing conveyed data collection and 3D inversion from a carbonate reservoir in Saudi Arabia Crosswell EM in Horizontal Wells. In Proceedings of the SEG New Orleans Annual Meeting, New Orleans, LA, USA, 18–23 November 2015; pp. 2848–2852.

16. Alpin, L. The Method of the Electric Logging in the Borehole with Casing. U.S. Patent 56,026, 30 November 1939.

17. Stewart, W. Electrical Logging Method and Apparatus. U.S. Patent 2,459,196, 18 January 1949.

18. Aulia, K.; Poernomo, B.; Richmond, W.; Wicaksono, A.; Beguin, P.; Benimili, D.; Dubourg, I.; Rouault, G.; VanderWal, P.; Boyd, A.; et al. Resistivity behind casing. *Oilfield Rev.* **2001**, *13*, 2–25.

19. Kaufman, A.A. The electrical field in a borehole with a casing. *Geophysics* **1990**, *55*, 29–38. [CrossRef]

20. Gyllensten, A.; Boyd, A. Cased Hole Formation Resistivity Tool Trial. In Proceedings of the SPE Middle East Oil Show, Manama, Bahrain, 17–20 March 2001.

21. Dorovsky, V.N.; Perepechko, Y.V.; Fedorov, A.I. Stoneley waves, radial waves, and method of measuring permeability and electroacoustic constant of saturated porous media. *Russ. Geol. Geophys.* **2013**, *54*, 237–245. [CrossRef]

22. Dorovsky, V. Electroacoustic Method of Conductivity Measurements through Casing. U.S. Patent 9,599,749, 21 March 2017.

23. Ripka, P. *Magnetic Sensors and Magnetometers*; Artech House Publishers: Norwood, MA, USA, 2001; p. 516.

24. Kudriavcev, A.; Saraev, Y. *Magnetic Susceptibility Logging*; St. Petersburg State University Publishing House: St. Petersburg, Russia, 2004; p. 270.

25. Yeltsov, I.; Eltsov, T.; Makarov, A.; Nikitenko, M. Effect of Dielectric Permittivity Distribution in Invaded Zone on Induction Log Data. In Proceedings of the International Conference "Mathematical and Information Technologies" (MIT-2016), Vrnjacka Banja, Serbia, 28–31 August 2016; pp. 66–67.

26. Eltsov, I.; Antonov, Y.; Makarov, A.; Kashevarov, A. Invaded zone evolution reconstructed from logging data. In Proceedings of the 2011 SEG Annual Meeting, San Antonio, TX, USA, 18–23 September 2011; pp. 509–513. [CrossRef]

27. Das, Y. Effects of soil electromagnetic properties on metal detectors. *IEEE Trans. Geosci. Remote Sens.* **2006**, *44*, 1444–1453. [CrossRef]

28. Barber, T.; Anderson, B.; Mowat, G. Using induction tools to identify magnetic formations and to determine relative magnetic susceptibility and dielectric constant. *Log Anal.* **1995**, *36*, 16–26.

29. Hu, G.D.; Geldmacher, I.M. The Effects of Magnetic Mud Invasion on Induction Logs. In Proceedings of the SEG Houston 2009 International Exposition and Annual Meeting, Houston, TX, USA, 25–30 October 2009; pp. 477–481.

30. Kaufman, A.A. *Theory of Induction Logging*; Nauka, SB RAS: Novosibirsk, Russia, 1965; p. 240.

31. Eltsov, T.; Nikitenko, M.; Terentyev, S. Fast algorithm for calculating the apparent resistivity. *Karotazhnik* **2013**, *228*, 63–72. (In Russian)

32. Frick, P.; Khripchenko, S.; Denisov, S.; Sokoloff, D.; Pinton, J. Effective magnetic permeability of a turbulent fluid. *Eur. Phys. J.* **2002**, *25*, 399–402. [CrossRef]

33. Sallehi, H. Characterization of Cement Paste in Fresh State Using Electrical Resistivity Technique. Ph.D. Thesis, Carleton University, Ottawa, ON, Canada, 2015.

34. Osterminski, K.; Polder, R.B.; Schießl, P. Long term behaviour of the resistivity of concrete. *Heron* **2012**, *57*, 211–230.